

# Safety-enhanced Human-Robot Interaction Control of Redundant Robot for Teleoperated Minimally Invasive Surgery

Hang Su<sup>1</sup>, Juan Sandoval<sup>2</sup>, Mohatahem Makhdoomi<sup>1</sup>, Giancarlo Ferrigno<sup>1</sup> and Elena De Momi<sup>1</sup>

**Abstract**—In this paper, a teleoperation control of a 7-DoF robot manipulator for Minimally Invasive Surgery (MIS), which guarantees a safety-enhanced compliant behavior in the null space, is described. The redundancy of the manipulator is exploited to provide a flexible workspace for nurses or other staff (assisting physicians, patient support). The issue with safety and accurate surgical task execution may arise in the presence of human-robot interaction. Based on the implemented impedance control of tele-operated MIS tasks, a safety enhanced constraint is applied on the compliant null space motion. At the same time, the control approach integrates an adaptive fuzzy compensator to guarantee the accuracy of the surgical tasks during the uncertain human-robot interaction. The performance of the proposed algorithm is verified with virtual surgical tasks. The results showed that the compliant null space motion is constrained in a safe area, and also that the accuracy of tool tip is improved, providing a flexible and safe collaborative behavior in the null space for human-robot interaction during surgical tasks.

## I. INTRODUCTION

Teleoperated robot-assisted surgery has been motivated by the advantages of greater surgical precision, increased range of motion, improved dexterity, and enhanced visualization for surgeons [1]. For Minimally Invasive Surgery (MIS), the end-effector of the manipulator must go through small incisions on the patient's body, which is commonly known as the Remote Center of Motion (RCM) constraint [2][3][4].

Redundancy of the serial manipulators can be exploited to achieve additional tasks, for example, obstacle avoidance [5], emotion conveyance [6], and manipulability optimization [7]. Redundancy can also provide flexible workspace with compliant motion behavior in the null-space for nurse or surgeon (assisting physicians, patient support) in a shared workspace. In [8], Sadeghian guarantees a correct task execution and a compliant behavior of the robot's body in case of accidental interaction in the null space. However, the compliant motion in the null space should be constrained in a feasible area without violation of the kinematic limits [9]. At the same time, the robot motion in the null space conflicts not only with humans' workspace, but also with other instruments and devices. Hence a safe constraint should be applied, when

the robot is close to kinematic limits or near collision, the compliant motion in the null space must be stopped.

Furthermore, in presence of uncertain disturbances during human-robot interaction, the accuracy of surgical tasks should be secured. Direct fuzzy adaptive controllers are known to work in the presence of a large uncertainty or unknown variation in plant parameters and disturbances [10]. In [11] and [12] unknown time-varying periodic disturbances from human-robot interaction are compensated by an adaptive fuzzy approximation.

In this paper, a safety-enhanced human-robot interaction control strategy is proposed for tele-operated MIS using a 7-DoF serial robot, providing safe and flexible solution for the robot and the medical staff in a shared workspace. The controller integrates three parts: a Cartesian compliance strategy, a safety-enhanced collaborative strategy in the null-space and a fuzzy adaptive compensator. The implemented Cartesian compliant strategy is exploited to execute the MIS tasks without violating the RCM constraint. The safety-enhanced collaborative strategy in the null-space is proposed to restrict the collaborative swivel motion in a safe range based on kinematic limits or an actual workspace situation in the operating room. An adaptive fuzzy compensator is introduced to work out the uncertain disturbances in the presence of human-robot interaction.

This paper is organized as follows: The system description of the proposed tele-operated MIS system is shown in Section II. The dynamic and kinematic model of the redundant manipulator, and the corresponding methodology are presented in Section III. In Section VI, the performance of the proposed control schemes is evaluated with real robot. And conclusions are drawn in Section V.

## II. SYSTEM DESCRIPTION

An overview of the developed tele-operated MIS system is shown in Fig. 1. A redundant robot (LWR4+, KUKA, Germany) is torque-controlled through the Fast Research Interface (FRI), which provides direct low-level real-time access to the robot controller (KRC) [13]. The tele-operation scheme implements a Cartesian position control for 3D coordinates with a master device (Sigma 7, Force Dimension, Switzerland) [14]. The orientation degrees of freedom of the end-effector are determined by the RCM constraint, as explained in Section III. The redundant DoF is exploited to provide a compliant human-robot interaction in the null space. For system validation, virtual surgical tasks in augmented reality are designed using a RGB 720p web camera

\*This work was supported by the European Unions Horizon 2020 research and innovation program under SMARTSurg project grant agreement No. 732515 and the China Scholarship Council.

<sup>1</sup>Hang Su, Mohatahem Makhdoomi, Giancarlo Ferrigno and Elena De Momi are with the Department of Electronics, Information and Bioengineering, Politecnico di Milano, 20133, Milan, Italy. hang.su, makhdoomi.mohatahem, giancarlo.ferrigno, elena.demomi@polimi.it

<sup>2</sup>Juan Sandoval is with PRISME Laboratory, University of Orleans, INSA CVL, France. juan.sandoval-arevalo@univ-orleans.fr

(Trust Trino) and an ArUco maker board [15]. The software system was developed with OROCOS (Open Robotic Control Software, <http://www.oroocos.org/>) application with a real-time Xenomai-patched Linux kernel and ROS (Robot Operating System, <http://www.ros.org/>) kinetic in Ubuntu. To secure the control frequency, the ROS vision node and the OROCOS torque controller were executed on separate computers with UDP communication between each other: the control loop was executed on the “control computer” and the vision ROS node was executed on the “vision computer”.

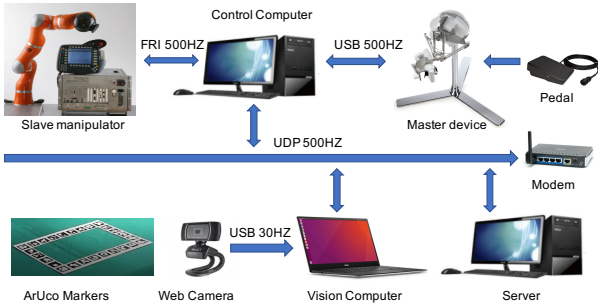


Fig. 1. Overview of the tele-operated surgical robot control system

### III. METHODOLOGY

#### A. Modelling the manipulator

1) *dynamic model*: The dynamic model of 7-DoF serial manipulator in the Lagrangian formulation can be expressed as:

$$\mathbf{M}(\mathbf{q})\ddot{\mathbf{q}} + \mathbf{C}(\mathbf{q}, \dot{\mathbf{q}})\dot{\mathbf{q}} + \mathbf{g}(\mathbf{q}) = \boldsymbol{\tau}_C - \boldsymbol{\tau}_{EXT} \quad (1)$$

where  $\mathbf{q} \in R^7$  is the joint values vector,  $\mathbf{M}(\mathbf{q}) \in R^{7 \times 7}$  is the inertia matrix,  $\mathbf{C}(\mathbf{q}, \dot{\mathbf{q}}) \in R^{7 \times 7}$  is a matrix representing the Coriolis and Centrifugal effects, and  $\mathbf{g}(\mathbf{q}) \in R^7$  is the vector of gravity torques. The torque vectors  $\boldsymbol{\tau}_C \in R^7$  and  $\boldsymbol{\tau}_{EXT} \in R^7$  represent the control torques and the external torque vectors, respectively. To control the tool tip, the torque controller solution can be defined as follows:

$$\boldsymbol{\tau}_C = \boldsymbol{\tau}_d + \hat{\mathbf{C}}(\mathbf{q}, \dot{\mathbf{q}})\dot{\mathbf{q}} + \hat{\mathbf{g}}(\mathbf{q}) + \hat{\boldsymbol{\tau}}_{EXT} \quad (2)$$

where  $\hat{\mathbf{C}}(\mathbf{q}, \dot{\mathbf{q}}) \in R^{7 \times 7}$  and  $\hat{\mathbf{g}}(\mathbf{q}) \in R^7$  are the estimated compensation terms,  $\hat{\boldsymbol{\tau}}_{EXT}$  is the filtered torque computed from external torque sensors, and  $\boldsymbol{\tau}_d$  is the control term introduced to achieve the desired tip pose.

2) *kinematic redundancy*: In this paper, the 6-DoFs of the end-effector were used to perform surgical tasks. In this case, the swivel motion of the robot arm in Fig. 2 can be viewed as the redundant motion in the null space [9]. However, as it is shown in Fig. 2, the motion range is constrained with joint limits. The feasible swivel area can be calculated with analytical kinematics [9].

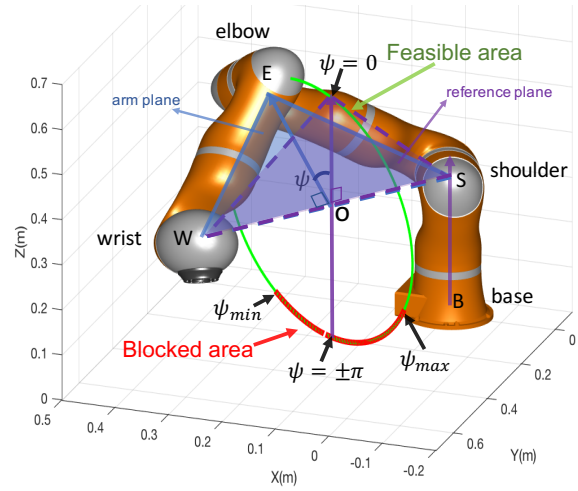


Fig. 2. Redundancy swivel solution. B, S, E and W are the base, shoulder, elbow and wrist joints, separately. O is the vertical intersection of OE and SW. The swivel angle  $\psi$  is defined by the angle between the reference plane (BSW) and the actual arm plane (SEW). The swivel angle can be calculated by:  $\psi = \text{sgn}((\vec{BS} \times \vec{SE}) \cdot \vec{SW}) \arccos\left(\frac{(\vec{BS} \times \vec{SE}) \cdot (\vec{SE} \times \vec{EW})}{\|\vec{BS} \times \vec{SE}\| \|\vec{SE} \times \vec{EW}\|}\right)$ , where  $\vec{BS}$  is the vector from the base to the shoulder,  $\vec{SE}$  is the vector from the shoulder to the elbow,  $\vec{SW}$  is the vector from the shoulder to the wrist and  $\vec{EW}$  is the vector from the elbow to the wrist. Its ideal swivel range is defined as  $[-\pi, \pi]$  including green part (feasible areas  $[\psi_{min}, \psi_{max}]$ ) and red part (blocked areas  $[-\pi, \psi_{min}]$  and  $(\psi_{max}, \pi]$ ).

#### B. Surgical task implementation

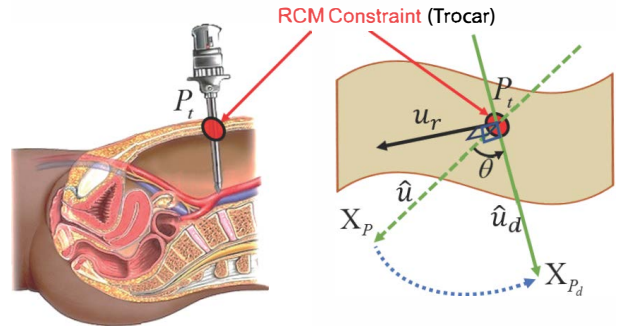


Fig. 3. Tele-operated MIS surgical scene: During the MIS, the tool-tip must go through the trocar position  $P_t$ , representing the RCM Constraint, where  $X_p$  and  $X_{p_d}$  are the actual and desired Cartesian position inside the abdomen,  $u_r$  is the rotation matrix from actual tip direction  $\hat{u}$  and desired tip direction  $\hat{u}_d$ , and  $\theta$  is the angle between  $\hat{u}$  and  $\hat{u}_d$ .

As it is shown in Fig. 3, the tool-tip trajectory and the RCM constraint must be simultaneously respected during the surgery. Given the desired Cartesian position from the master device, an online pose planning scheme is introduced.

The operational coordinates  $\mathbf{X} = [\mathbf{X}_P, \mathbf{X}_R]^T \in R^6$  are the actual tip pose, including the actual tool-tip position  $\mathbf{X}_P = [x, y, z]$  and the actual tool orientation with Euler angle expressed by  $\mathbf{X}_R = [\alpha, \beta, \gamma]$ .  $\mathbf{X}_d = [\mathbf{X}_{P_d}, \mathbf{X}_{R_d}] \in R^6$  is the desired tip pose, where  $\mathbf{X}_{P_d} = [x_d, y_d, z_d]$  is the desired Cartesian position given by the master device and the desired orientation  $\mathbf{X}_{R_d} = [\alpha_d, \beta_d, \gamma_d]$  is calculated based on  $\mathbf{X}_P$  online in order to guarantee the tip going through the trocar position  $\mathbf{P}_t = [x_t, y_t, z_t]$  during the teleoperation, as follows:

The rotation angle  $\theta$  (see Fig. 3) between the actual tool direction  $\hat{\mathbf{u}}$  and the desired tool direction  $\hat{\mathbf{u}}_d$  can be calculated as  $\theta = \arctan \frac{\hat{\mathbf{u}}_d \times \hat{\mathbf{u}}}{\hat{\mathbf{u}}_d \cdot \hat{\mathbf{u}}}$ . The unit vector describing the rotation axis  $\mathbf{u}_r = [u_x, u_y, u_z]$  from  $\hat{\mathbf{u}}$  to  $\hat{\mathbf{u}}_d$  is defined by  $\mathbf{u}_r = \frac{\hat{\mathbf{u}}_d \times \hat{\mathbf{u}}}{\|\hat{\mathbf{u}}_d \times \hat{\mathbf{u}}\|}$ . A Skew-symmetric matrix is introduced as:

$$\mathbf{\Gamma} = \begin{bmatrix} 0 & -u_z & u_y \\ u_z & 0 & u_x \\ -u_y & u_x & 0 \end{bmatrix}$$

Finally, the desired orientation can be calculated using:

$$\mathbf{R}_d = \mathbf{I} + \mathbf{\Gamma} \sin(\theta) + 2\mathbf{\Gamma}^2 \sin^2\left(\frac{\theta}{2}\right) \cdot \mathbf{R} \quad (3)$$

where  $\mathbf{R}$  and  $\mathbf{R}_d$  are the actual and the desired rotation matrix, respectively.  $\mathbf{X}_{R_d}$  can be computed from Euler transformation of the rotation matrix  $\mathbf{R}_d$ . To reach the desired tip pose  $\mathbf{X}_d$ , a Cartesian compliance control term,  $\tau_T \in \mathbf{R}^7$ , is introduced as

$$\tau_T = \mathbf{J}^T \mathbf{F}_T = \mathbf{J}^T \left( \frac{\partial \mathbf{V}(\mathbf{q})}{\partial \mathbf{X}} \right)^T - \mathbf{D}_x \dot{\mathbf{X}} \quad (4)$$

based on the potential function of a virtual spring and a damping term, as used in [16], where  $\mathbf{J} \in \mathbf{R}^{6 \times 7}$  is the Jacobian matrix,  $\mathbf{D}_x \in \mathbf{R}^{6 \times 6}$  is the diagonal damping matrix, and the virtual potential function  $\mathbf{V}(\mathbf{q}) \in \mathbf{R}$  is defined based on the difference between the desired and the actual Cartesian trajectory  $\tilde{\mathbf{X}}(\mathbf{q}) = \mathbf{X}_d - \mathbf{X}(\mathbf{q})$ , as follows:

$$\mathbf{V}(\mathbf{q}) = \frac{1}{2} \tilde{\mathbf{X}}(\mathbf{q})^T \mathbf{K}_x \tilde{\mathbf{X}}(\mathbf{q}) \quad (5)$$

where  $\mathbf{X}(\mathbf{q})$  is the actual target pose calculated from forward kinematic function,  $\mathbf{K}_x \in \mathbf{R}^{6 \times 6}$  is the diagonal stiffness matrix. For simplification, we assume that the surgical robot is far away from its singularity and the pseudoinverse of  $\mathbf{J}$  exists.

### C. Safety enhanced compliant strategy in the null space

If necessary, the nurses can move the robot arm by hand to get free workspace, as it is shown in Fig. 4. However, it should also avoid the known fixed physical objects existing in the robot's workspace. For example, it is dangerous to move the swivel motion near the blocked swivel area or hit other medical devices. Hence, a safe swivel motion constraint area  $[\psi_{minf}, \psi_{maxf}]$  is defined, which can be defined according to the actual situation in the operating room. The assumed safe constraint area  $[\psi_{minf}, \psi_{maxf}]$  belongs to the feasible swivel area  $[\psi_{min}, \psi_{max}]$  in Fig. 2.

To constrain the swivel motion in the safe area, a virtual force  $\mathbf{F}_\psi = \mathbf{u}_{F_\psi} \cdot \|\mathbf{F}_\psi\|$  will be activated to prevent the swivel motion near the constraint boundary. The direction vector  $\mathbf{u}_{F_\psi}$  of  $\mathbf{F}_\psi$  is perpendicular to the robot arm plane (BSW), expressed by

$$\mathbf{u}_{F_\psi} = \text{sgn}\left(\frac{\psi_{minf} + \psi_{maxf}}{2} - \psi\right) \cdot \frac{\mathbf{S}\vec{E} \times \mathbf{E}\vec{W}}{\|\mathbf{S}\vec{E} \times \mathbf{E}\vec{W}\|} \quad (6)$$

where  $\psi$  is the actual swivel angle,  $\mathbf{S}\vec{E}$  is the vector from the shoulder to the elbow in Fig. 2, and  $\mathbf{E}\vec{W}$  is the vector from

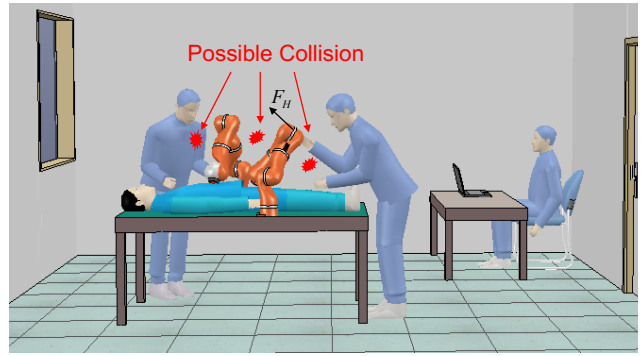


Fig. 4. Safety enhanced strategy in the null space: 1) To provide flexible workspace for the medical staff, the swivel motion should be freely moved with hand force  $\mathbf{F}_H$ . 2) The swivel motion range should be constrained to avoid kinematic limits and the possible collision in workspace, which could be set based on the actual situation in the operating room.

the elbow to the wrist. The virtual force  $F_\psi$  can be expressed as:

$$\mathbf{F}_\psi = \begin{cases} \mathbf{u}_{F_\psi} \cdot (k_\psi(\psi_{minf} + \rho - \psi) - d_\psi \dot{\psi}) & \psi < \psi_{minf} \\ \mathbf{u}_{F_\psi} \cdot (k_\psi(\psi_{maxf} - \rho - \psi) - d_\psi \dot{\psi}) & \psi > \psi_{maxf} \\ 0 & [\psi_{minf}, \psi_{maxf}] \end{cases}$$

where  $\rho \in \mathbf{R}$  is a positive constant threshold value to avoid the violation of the swivel constraint,  $k_\psi$  and  $d_\psi$  are the constant coefficients.

Then the corresponding null-space projected torque,  $\tau_N \in \mathbf{R}^7$ , generated from  $\mathbf{F}_\psi$ , is calculated as follows:

$$\tau_N = \mathbf{N}(\mathbf{q}) \cdot (\mathbf{J}_e^T \mathbf{F}_\psi - \hat{\tau}_{EXT}) \quad (7)$$

where  $\mathbf{J}_e \in \mathbf{R}^{3 \times 7}$  is the Jacobian matrix between the robot base and the elbow,  $\mathbf{N}(\mathbf{q}) \in \mathbf{R}^{7 \times 7}$  represents the null-space projector calculated using the inertia-weighted pseudo-inverse matrix  $\mathbf{J}(\mathbf{q})_M^+$  [17], given by:

$$\mathbf{N}(\mathbf{q}) = \mathbf{I} - \mathbf{J}(\mathbf{q})^T (\mathbf{J}(\mathbf{q})_M^+)^{-1} \quad (8)$$

### D. Fuzzy adaptive compensation for uncertain disturbance with human-robot interaction

Since the hand force  $\mathbf{F}_H$  applied on the robot arm in Fig. 4 is uncertain and time-variable, the influence of human-robot interaction on the surgical tip is uncertain. The filtered external torques,  $\hat{\tau}_{EXT}$ , are not accurate enough to estimate the hand force,  $\mathbf{F}_H$ , in the real application. There is still an uncertain bounded error in the estimated terms  $\hat{\mathbf{C}}(\mathbf{q}, \dot{\mathbf{q}})$  and  $\hat{\mathbf{g}}(\mathbf{q})$ , which has an influence on the accuracy. Constant coefficients  $\mathbf{K}_x$  and  $\mathbf{D}_x$  cannot handle the uncertain disturbance. Adaptive nonlinear controller can compensate the unknown time-varying periodic disturbances from human-robot interaction [18]. During the surgery, the desired Cartesian position is achieved by the Cartesian position of the tool tip and the RCM constraint is performed by the orientation of the tool tip. In this case, 6 degrees of freedom of the tool tip are adopted to secure the surgical task. To secure the surgical task accuracy is as securing the accuracy of the end-effector. The total of unknown and time-varying disturbance on the tool tip can be assumed as  $\mathbf{s}(\mathbf{q}, \dot{\mathbf{q}}) \in \mathbf{R}^6, \exists \epsilon_1, \epsilon_2 \in \mathbf{R}^+, \forall t >$

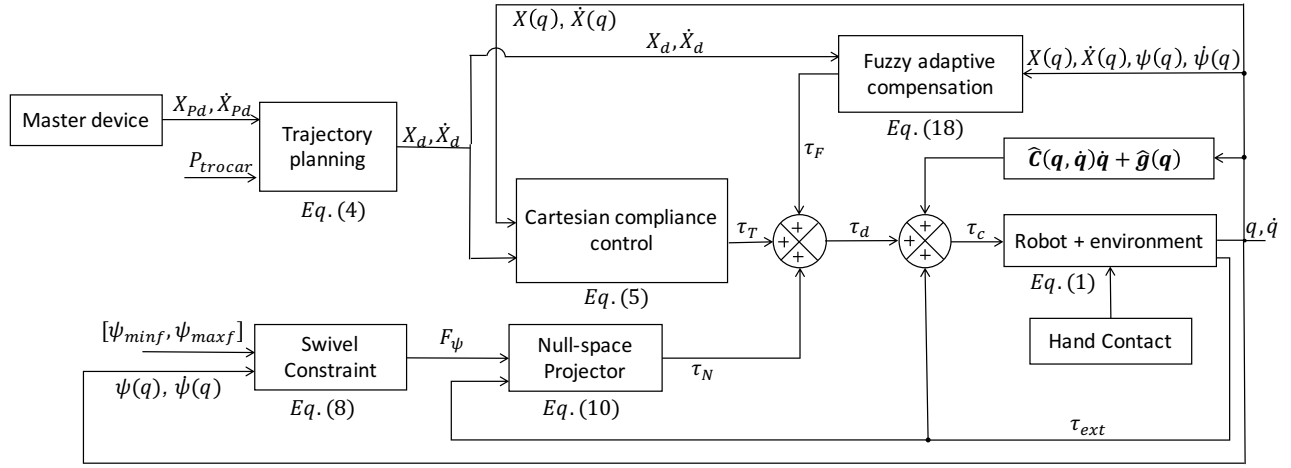


Fig. 5. Block diagram representing the proposed control architecture: The “Trajectory planning” block is used to calculate the desired end-effector pose  $\mathbf{X}_d$  to respect the RCM constraint, the “Cartesian compliance controller” calculates the torque  $\tau_T$  to achieve the desired pose of the end effector, the “Swivel Constraint” calculates the virtual force applied on the null space, the “Null-space Projector” maps the virtual force to joints torque, the “Fuzzy Adaptive Compensation” compensates the unknown disturbance, “Robot and environment” and “Hand Contact” are robot arm dynamic model and uncertain human-robot interaction.

$0, \|\mathbf{s}(\mathbf{q}, \dot{\mathbf{q}})\| \leq \epsilon_1, \|\dot{\mathbf{s}}(\mathbf{q}, \dot{\mathbf{q}})\| \leq \epsilon_2$ . When it is mapped to the joints space, the dynamic model can be rewritten by

$$\mathbf{M}(\mathbf{q})\ddot{\mathbf{q}} + \mathbf{C}(\mathbf{q}, \dot{\mathbf{q}})\dot{\mathbf{q}} + \mathbf{g}(\mathbf{q}) + \mathbf{J}^T \mathbf{s}(\mathbf{q}, \dot{\mathbf{q}}) = \tau_C - \tau_{EXT} \quad (9)$$

In [9], if not in singularity, there is a unique mapping relation between joint angles  $\mathbf{q}$  and tip-pose  $\mathbf{X}$  when there is a fixed swivel angle  $\psi : \mathbf{q} = \chi(\mathbf{X}, \psi)$ . The joints speed  $\dot{\mathbf{q}}$  is equal to  $\frac{\partial \chi(\mathbf{X}, \psi)}{\partial \mathbf{X}} + \frac{\partial \chi(\mathbf{X}, \psi)}{\partial \psi} = \mathbf{\Gamma}(\mathbf{X}, \dot{\mathbf{X}}, \psi, \dot{\psi})$ . Hence the uncertain term  $\mathbf{s}(\mathbf{q}, \dot{\mathbf{q}})$  can be reexpressed as:

$$\mathbf{s}(\mathbf{q}, \dot{\mathbf{q}}) = \mathbf{F}(\mathbf{X}, \dot{\mathbf{X}}, \psi, \dot{\psi}) \quad (10)$$

Since  $\mathbf{F}(\mathbf{X}, \dot{\mathbf{X}}, \psi, \dot{\psi})$  is a new complicated function without detailed expression, in this paper, a multi-input and multi-output (MIMO) adaptive fuzzy compensator will be employed to approximate  $\mathbf{F}(\mathbf{X}, \dot{\mathbf{X}}, \psi, \dot{\psi})$ . The approximation of the function  $\mathbf{F} : \mathbf{R}^{14} \rightarrow \mathbf{R}^6$  can be represented as follows

$$\mathbf{F}(\mathbf{X}, \dot{\mathbf{X}}, \psi, \dot{\psi}) = \mathbf{\Theta} \xi(\mathbf{X}, \dot{\mathbf{X}}, \psi, \dot{\psi}) \quad (11)$$

where  $\mathbf{\Theta} = [\theta_1, \theta_2, \dots, \theta_6]^T \in \mathbf{R}^{6 \times 7}$  is the weight parameter matrix,  $\theta_i \in \mathbf{R}^{7 \times 1}$  ( $i = 1, \dots, 6$ ) and  $\xi(\mathbf{X}, \dot{\mathbf{X}}, \psi, \dot{\psi}) = [\xi_1, \xi_2, \dots, \xi_7] \in \mathbf{R}^{7 \times 1}$ ,  $\xi_j \in \mathbf{R}$  ( $j = 1, \dots, 7$ ) is the basic functions:

$$\xi_j = \frac{\prod_{l=1}^{14} \mu_{F_l^j(x_l)}}{\sum_{j=1}^7 \prod_{l=1}^{14} \mu_{F_l^j(x_l)}} \quad (12)$$

where  $x_{1,2,\dots,14} = [x, y, z, \alpha, \beta, \gamma, \dot{x}, \dot{y}, \dot{z}, \dot{\alpha}, \dot{\beta}, \dot{\gamma}, \psi, \dot{\psi}]$ , and  $\mu_{F_l^j(x_l)} \in \mathbf{R}$  is the adaptive membership functions defined as follows:

$$\begin{cases} \mu_{F_1^1(x_1)} = \frac{1}{1 + \exp(5(x_1 + 0.6))} \\ \mu_{F_1^2(x_1)} = \exp(-0.5(x_1 + 0.4)^2) \\ \mu_{F_1^3(x_1)} = \exp(-0.5(x_1 + 0.2)^2) \\ \mu_{F_1^4(x_1)} = \exp(-0.5x_1^2) \\ \mu_{F_1^5(x_1)} = \exp(-0.5(x_1 - 0.2)^2) \\ \mu_{F_1^6(x_1)} = \exp(-0.5(x_1 - 0.4)^2) \\ \mu_{F_1^7(x_1)} = \frac{1}{1 + \exp(-5(x_1 - 0.6))} \end{cases}$$

The adaptive control law [19] to adjust the weight parameters  $\mathbf{\Theta}$  is chosen as  $\dot{\mathbf{\Theta}} = [\dot{\theta}_1, \dot{\theta}_2, \dots, \dot{\theta}_6] \in \mathbf{R}^{6 \times 7}$ ,  $\theta_i \in \mathbf{R}^{7 \times 1}$ ,  $i = 1, 2, \dots, 6$ :

$$\dot{\mathbf{\Theta}} = \gamma \mathbf{E} \mathbf{P} \xi^T(\mathbf{X}, \dot{\mathbf{X}}, \psi, \dot{\psi}) \quad (13)$$

where  $\gamma \in \mathbf{R}^{6 \times 6}$  is a diagonal matrix determining the updating speed,  $\mathbf{E} = [\mathbf{X}_d - \mathbf{X}(\mathbf{q}), -\dot{\mathbf{X}}(\mathbf{q})]^T$  is the pose error of the tool tip, and  $\mathbf{P} \in \mathbf{R}^{2 \times 1}$  is the last column of a symmetric positive definite matrix based on Lyapunov’s stability theory [10].

After approximation of the uncertain disturbance on the end-effector, an adaptive fuzzy term  $\tau_F \in \mathbf{R}^7$

$$\tau_F = -\mathbf{J}^T \mathbf{F}(\mathbf{X}, \dot{\mathbf{X}}, \psi, \dot{\psi}) = -\mathbf{J}^T \mathbf{\Theta} \xi(\mathbf{X}, \dot{\mathbf{X}}, \psi, \dot{\psi}) \quad (14)$$

is introduced to compensate the uncertain human-robot interaction.

The overview of proposed safety enhanced control block diagram is shown in Fig. 5. The desired control term can be expressed as:

$$\tau_d = \tau_T + \tau_N + \tau_F \quad (15)$$

TABLE I  
EXPERIMENTAL CONTROLLER PARAMETERS

| Controller                          | Controller parameters   |
|-------------------------------------|---|
| $\tau_d = \tau_T$                   | $\mathbf{K}_x = \text{diag}[3000, 3000, 3000, 300, 300, 300]$<br>$\mathbf{D}_x = \text{diag}[30, 30, 30, 3.5, 3.5, 3.5]$  |
| $\tau_d = \tau_T + \tau_N + \tau_F$ | $\mathbf{K}_x = \text{diag}[3000, 3000, 3000, 300, 300, 300]$<br>$\mathbf{D}_x = \text{diag}[30, 30, 30, 3.5, 3.5, 3.5]$<br>$k_\psi = 150.0, d_\psi = 5.0, \rho = 0.06$<br>$\gamma = \text{diag}[0.3, 0.3, 0.3, 0.03, 0.03, 0.03]$<br>$\mathbf{P} = \text{diag}[14, 2]$ |

#### IV. RESULTS

Two healthy subjects (One teleoperator (male, 28 years old), and one medical staff (male, 27 years old)) were enrolled to setup the experimental scene. The whole procedure

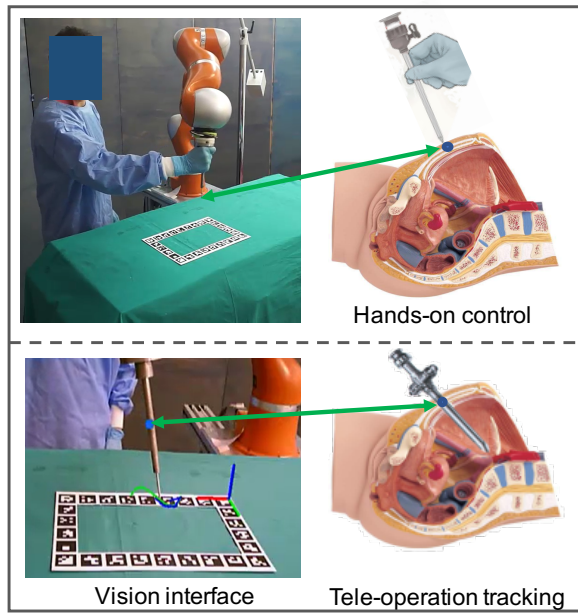


Fig. 6. Operative procedure: 1) Hands-on control ( $\tau_d = [0, 0, 0, 0, 0, 0, 0]^T$ ) is activated to locate trocar position (small incision on the patient body); 2) Tele-operation tracking is to control the tip tracking the virtual surgical tasks in augmented reality. The size of designed tasks are around  $8.0cm \times 15.0cm$  on the horizontal plane, which is similar to the actual MIS task. The vision interface displayed the camera images, RCM constraint, desired task path, actual tip drawn paths on the display.

can be seen in Fig. 6: firstly, the medical staff locate the small incision on the patient body and then the teleoperator use the master device to control tool tip tracking the surgical tasks. The tool tip should always go through the blue point (trocar) during the teleoperation. At the same time, the medical staff is free to move the robot arm in an allowed swivel area.

To evaluate the proposed control method, the Cartesian position error,  $\mathbf{E}_{X_p}$ , and the RCM constraint error,  $\mathbf{E}_{P_t}$ , are recorded during the whole experiment:

$$\mathbf{E}_{X_p} = \|\mathbf{X}_{p_d} - \mathbf{X}_p\| \quad (16)$$

$$\mathbf{E}_{P_t} = \|(\mathbf{P}_t - \mathbf{X}_p) \times \hat{\mathbf{u}}_c\| \quad (17)$$

where  $\hat{\mathbf{u}}_c$  is actual tip unit direction vector. The corresponding coefficients table can be found in Table I. Firstly, comparison of performance between safety enhanced control strategy (SECS)  $\tau_d = \tau_T + \tau_N + \tau_F$  and only cartesian compliance control (CCC)  $\tau_d = \tau_T$  were conducted on the fixed end-effector pose. Secondly, to validate the feasibility of the proposed strategy for general teleoperated MIS, the SECS controller is conducted with teleoperation tracking.

Fig. 7 shows the comparison of the two controllers with the same desired cartesian position and RCM constraint. The CCC was applied firstly and then the SECS was switched online. Fig.7 (a) shows the swivel motion  $\psi$  with the human-robot interaction. Fig. 7 (b) shows the magnitude of virtual force  $\mathbf{F}_\psi$  applied on the elbow to constrain the swivel motion. The online Cartesian position error is shown in Fig. 7 (c) and the online RCM constraint error is in Fig.7 (d). It is easy

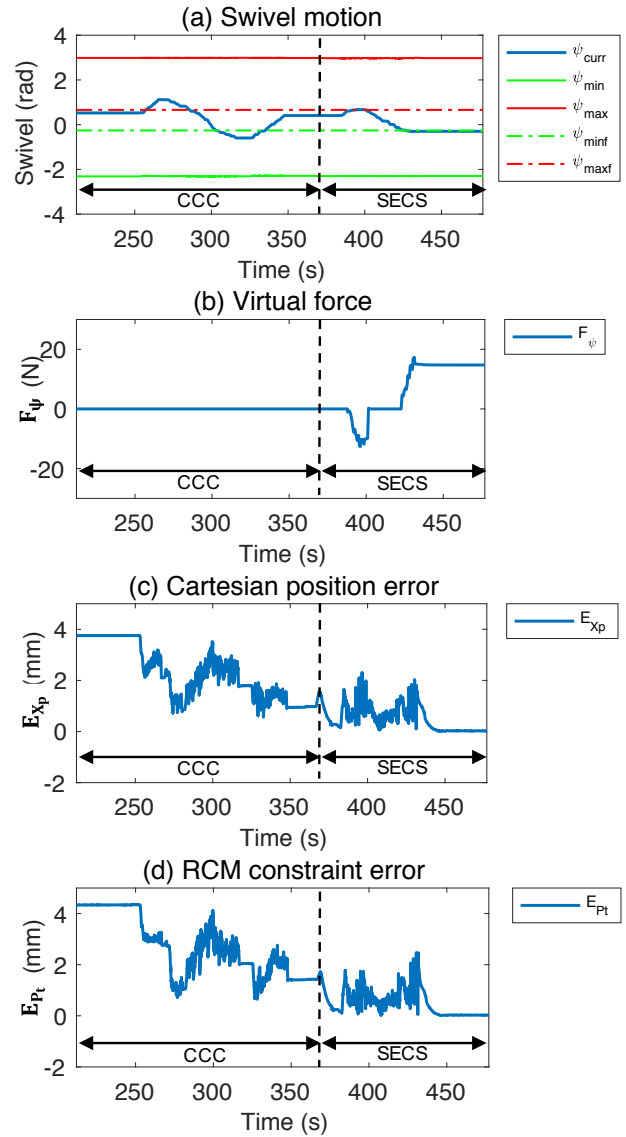


Fig. 7. Comparison between CCC  $\tau_d = \tau_T$  and SECS  $\tau_d = \tau_T + \tau_N + \tau_F$

to see that the safety enhanced strategy can constrain the swivel boundary in a safe area  $[\psi_{minf}, \psi_{maxf}]$  with the virtual force  $\mathbf{F}_\psi$ . Furthermore, the online Cartesian error and RCM constraint error converges to zero.

Fig. 8 shows the performance of the proposed safety enhanced strategy on the teleoperation tracking tasks. The SECS was applied during the whole procedure to track three different desired curve tasks. As it is shown in Fig. 8, virtual task paths were designed in vision interface for teleoperation tracking with different shapes: (I) Half ellipse curve, (II) Sine curve and (III) Triangle curve. Fig.8 (a) shows the swivel motion  $\psi$  with the human-robot interaction. Fig. 8 (b) shows the magnitude of virtual force  $\mathbf{F}_\psi$  applied on the elbow to constrain the swivel motion. The online Cartesian position error is shown in Fig. 8 (c) and the online RCM constraint error is in Fig. 8 (d). It is obvious that the safety enhanced

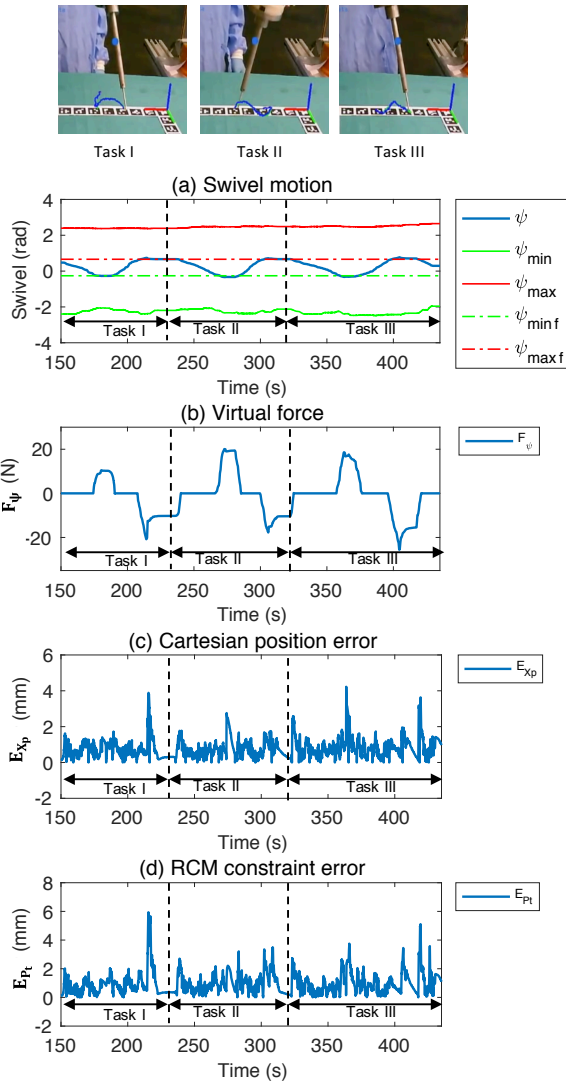


Fig. 8. Performance on the teleoperation tracking tasks with SECS  $\tau_d = \tau_T + \tau_N + \tau_F$

strategy can constrain the swivel motion in a safe area and the online Cartesian error and RCM error are bounded and stable.

## V. DISCUSSION AND CONCLUSION

This paper developed a safety enhanced human-robot interaction control scheme for teleoperated MIS integrating three parts: 1) Cartesian compliance control involving the main MIS surgical task implementation, 2) null-space constraint providing a flexible and safe human-robot interaction undergoing surgery, 3) fuzzy adaptive compensation working out the uncertain and time-varying disturbance. Experimental evaluations were conducted with virtual surgical tasks to validate the performance. The results show that the proposed control algorithm not only can constrain the compliant null space motion in a safe area, also can compensate the uncertain and time-varying disturbance existing in the system, securing the quality of the surgery. Compared with other achieved compliant behaviour in null space [8], the proposed

metod apply a safe area to make it more safe for real application. However, the experiment is only conducted with virtual tasks in augmented reality. The future work will try to verify and optimize its performance with real phantom, involving more complicated dynamic interaction.

## REFERENCES

- [1] A. R. Lanfranco, A. E. Castellanos, J. P. Desai, and W. C. Meyers, "Robotic surgery: a current perspective," *Annals of surgery*, vol. 239, no. 1, p. 14, 2004.
- [2] R. C. Locke and R. V. Patel, "Optimal remote center-of-motion location for robotics-assisted minimally-invasive surgery," in *Robotics and Automation, 2007 IEEE International Conference on*. IEEE, 2007, pp. 1900–1905.
- [3] N. Aghakhani, M. Geravand, N. Shahrari, M. Vendittelli, and G. Oriolo, "Task control with remote center of motion constraint for minimally invasive robotic surgery," in *Robotics and Automation (ICRA), 2013 IEEE International Conference on*. IEEE, 2013, pp. 5807–5812.
- [4] E. De Momi and G. Ferrigno, "Robotic and artificial intelligence for keyhole neurosurgery: the robocast project, a multi-modal autonomous path planner," *Proceedings of the Institution of Mechanical Engineers, Part H: Journal of Engineering in Medicine*, vol. 224, no. 5, pp. 715–727, 2010.
- [5] M. D. Comporetti, E. De Momi, A. Vaccarella, M. Riechmann, and G. Ferrigno, "Optically tracked multi-robot system for keyhole neurosurgery," in *Robotics and Automation (ICRA), 2011 IEEE International Conference on*. IEEE, 2011, pp. 661–666.
- [6] J.-A. Claret, G. Venture, and L. Basañez, "Exploiting the robot kinematic redundancy for emotion conveyance to humans as a lower priority task," *International journal of social robotics*, vol. 9, no. 2, pp. 277–292, 2017.
- [7] L. Jin, S. Li, H. M. La, and X. Luo, "Manipulability optimization of redundant manipulators using dynamic neural networks," *IEEE Transactions on Industrial Electronics*, 2017.
- [8] H. Sadeghian, L. Villani, M. Keshmiri, and B. Siciliano, "Task-space control of robot manipulators with null-space compliance," *IEEE Transactions on Robotics*, vol. 30, no. 2, pp. 493–506, 2014.
- [9] M. Shimizu, H. Kakuya, W.-K. Yoon, K. Kitagaki, and K. Kosuge, "Analytical inverse kinematic computation for 7-dof redundant manipulators with joint limits and its application to redundancy resolution," *IEEE Transactions on Robotics*, vol. 24, no. 5, pp. 1131–1142, 2008.
- [10] L.-X. Wang, "Stable adaptive fuzzy control of nonlinear systems," *IEEE Transactions on fuzzy systems*, vol. 1, no. 2, pp. 146–155, 1993.
- [11] H. Su, H. Zhang, Z. Li, and C.-Y. Su, "Adaptive fuzzy control of operation space constrained exoskeletons under unmodelled dynamics," in *Intelligent Control and Automation (WCICA), 2014 11th World Congress on*. IEEE, 2014, pp. 3277–3282.
- [12] Z. Li, C.-Y. Su, G. Li, and H. Su, "Fuzzy approximation-based adaptive backstepping control of an exoskeleton for human upper limbs," *IEEE Transactions on Fuzzy Systems*, vol. 23, no. 3, pp. 555–566, 2015.
- [13] G. Schreiber, A. Stemmer, and R. Bischoff, "The fast research interface for the kuka lightweight robot," in *IEEE Workshop on Innovative Robot Control Architectures for Demanding (Research) Applications How to Modify and Enhance Commercial Controllers (ICRA 2010)*, 2010, pp. 15–21.
- [14] N. ENAYATI, "Adaptive shared-control in surgical robotics," 2017.
- [15] S. Garrido-Jurado, R. Muñoz-Salinas, F. J. Madrid-Cuevas, and M. J. Marín-Jiménez, "Automatic generation and detection of highly reliable fiducial markers under occlusion," *Pattern Recognition*, vol. 47, no. 6, pp. 2280–2292, 2014.
- [16] A. Dietrich, T. Wimbock, A. Albu-Schaffer, and G. Hirzinger, "Integration of reactive, torque-based self-collision avoidance into a task hierarchy," *IEEE Transactions on Robotics*, vol. 28, no. 6, pp. 1278–1293, 2012.
- [17] O. Khatib, "A unified approach for motion and force control of robot manipulators: The operational space formulation," *IEEE Journal on Robotics and Automation*, vol. 3, no. 1, pp. 43–53, 1987.
- [18] H. Su, Z. Li, G. Li, and C. Yang, "Emg-based neural network control of an upper-limb power-assist exoskeleton robot," in *International Symposium on Neural Networks*. Springer, 2013, pp. 204–211.
- [19] B. Chen, X. P. Liu, S. S. Ge, and C. Lin, "Adaptive fuzzy control of a class of nonlinear systems by fuzzy approximation approach," *IEEE Transactions on Fuzzy Systems*, vol. 20, no. 6, pp. 1012–1021, 2012.